

Enantioselective Orientation of Chiral Molecules Induced by Terahertz Pulses with Twisted Polarization

Ilia Tutunnikov,^{1,*} Long Xu,^{1,*} Robert W. Field,^{2,†} Keith A. Nelson,^{2,‡} Yehiam Prior,^{1,§} and Ilya Sh. Averbukh^{1,¶}

¹*AMOS and Department of Chemical and Biological Physics,
The Weizmann Institute of Science, Rehovot 7610001, Israel*

²*Department of Chemistry, Massachusetts Institute of Technology, Cambridge, MA 02139, USA*

Chirality and chiral molecules are key elements in modern chemical and biochemical industries. Individual addressing, and the eventual separation of chiral enantiomers has been and still is an important elusive task in molecular physics and chemistry, and a variety of methods has been introduced over the years to achieve this goal. Here, we theoretically demonstrate that a pair of cross-polarized THz pulses interacting with chiral molecules through their permanent dipole moments induces an enantioselective orientation of these molecules. This orientation persists for a long time, exceeding the duration of the THz pulses by several orders of magnitude, and its dependency on temperature and pulses' parameters is investigated. The persistent orientation may enhance the deflection of the molecules in inhomogeneous electromagnetic fields, potentially leading to viable separation techniques.

I. INTRODUCTION

Molecular chirality was discovered in the 19th century by Louis Pasteur [1] (for a historical excursion, see e.g. [2]), and since then chirality has attracted considerable interest owing to its importance in physics, chemistry, biology, and medicine. Chiral molecules exist in two forms, called left-, and right-handed enantiomers, which are mirror images of each other and cannot be superimposed by translations or rotations [3]. Even though the two enantiomers have many identical chemical and physical properties, e.g. boiling points and moments of inertia, they often differ in their biological activities. This is only one of the reasons why the abilities to differentiate, selectively manipulate, and separate the enantiomers in mixtures containing both of them are of great practical importance. From the point of view of fundamental physics, chiral molecules seem to be promising candidates for experiments aimed at measuring parity violation effects [4].

Some of the physical properties of the two enantiomers mimic their reflection relation. For example, the product of three Cartesian components of the molecular dipole moment has the opposite sign for the two enantiomers [5]. Utilizing the distinct properties of the enantiomers, a variety of methods for chiral discrimination using electromagnetic fields has been developed over the years, including: microwave three-wave mixing spectroscopy [5–10], photoelectron circular dichroism [11–15], Coulomb explosion imaging [16–18], and high-order harmonic generation [19]. Most recently, a generic purely optical method for enantioselective *orientation* has been proposed [20–23] and experimentally demonstrated on propylene oxide

molecule spun by an optical centrifuge [24] in which the polarization vector rotates unidirectionally with increasing angular velocity. This last method utilizes laser fields with “twisted” polarization [see Fig. 1(a)] and relies on the off-diagonal elements of the polarizability tensor which, in chiral molecules, have opposite signs for the two enantiomers. In related works, it was demonstrated that the optically induced orientation persists long after the end of the laser pulses [23, 25]. For the purpose of the current work, fields with twisted polarization are understood to include: pairs of delayed cross-polarized pulses [26–28] [see Fig. 1(b)], chiral pulse trains [29, 30], polarization-shaped pulses [31–35], and the aforementioned optical centrifuge for molecules [36–40].

In this work, we study the orientation of chiral molecules induced by terahertz (THz) pulses with twisted polarization. Since the advent of THz pulse technology, intense THz pulses have been exploited for producing transient field-free orientation of polar molecules of various complexity [41–47]. Although transient orientation revival spikes may periodically appear on long time scales, the orientation signature generally rides on a zero baseline and its time average is exactly zero. Recently, it was shown that a single linearly polarized THz pulse induces persistent orientation in symmetric- and asymmetric-top molecules, including chiral molecules [48]. In contrast to the transient signal, persistent orientation means that the time-averaged post-pulse orientation degree differs from zero on a long time scale, in the case discussed in this paper - exceeding the duration of the THz pulse by several orders of magnitude.

Here, we theoretically demonstrate that when applied to *chiral molecules*, a *pair of time-delayed cross-polarized THz pulses* induces orientation in a direction perpendicular to the plane spanned by the polarizations. The orientation is enantioselective, meaning that the two enantiomers are oriented in opposite directions relative to the plane. We show that the time-averaged projections of the molecular dipole moment onto all three laboratory axes

* These authors contributed equally to this work.

† rwfield@mit.edu

‡ kanelson@mit.edu

§ yehiam.prior@weizmann.ac.il

¶ ilya.averbukh@weizmann.ac.il

remains nonzero on a nanosecond timescale. The paper is organized as follows. In Sec. II, we briefly summarize our theoretical methods. In Sec. III, we present and analyze the results of classical and fully quantum simulations of THz field-driven molecular rotational dynamics, and Section IV concludes the presentation.

II. METHODS

We carried out classical as well as fully quantum mechanical simulations of the THz field-driven rotational dynamics of chiral molecules. This section outlines the theoretical approaches used in both cases.

Quantum simulation. The Hamiltonian describing the molecular rotation driven by a THz field interacting with the molecular dipole moment is given by [49, 50]

$$\hat{H}(t) = \hat{H}_r + \hat{H}_{\text{int}}(t), \quad (1)$$

where \hat{H}_r is the rotational kinetic energy Hamiltonian and $\hat{H}_{\text{int}}(t) = -\hat{\boldsymbol{\mu}} \cdot \mathbf{E}(t)$ is the molecule-field interaction. Here $\hat{\boldsymbol{\mu}}$ is the molecular dipole moment operator and $\mathbf{E}(t)$ is the external electric field. In this work, the contributions of higher order interaction terms are small, and are not included. For the quantum mechanical treatment, it is convenient to express the Hamiltonian in the basis of field-free symmetric-top wave functions $|JKM\rangle$ [51]. Here J is the value of the total angular momentum (in units of \hbar), while K and M are the values of the projections on the molecule-fixed axis (here the axis with smallest moment of inertia) and the laboratory-fixed Z axis, respectively. The nonzero matrix elements of the asymmetric-top kinetic energy operator are given by [51]

$$\langle JKM|\hat{H}_r|JKM\rangle = \frac{B+C}{2} [J(J+1) - K^2] + AK^2, \quad (2)$$

$$\langle JKM|\hat{H}_r|J, K \pm 2, M\rangle = \frac{B-C}{4} f(J, K \pm 1), \quad (3)$$

where $f(J, K) = \sqrt{(J^2 - K^2)[(J+1)^2 - K^2]}$, $A = \hbar^2/2I_a$, $B = \hbar^2/2I_b$, $C = \hbar^2/2I_c$ are the rotational constants ($A > B > C$), and $I_a < I_b < I_c$ are the molecular moments of inertia. The time-dependent Schrödinger equation $i\hbar\partial_t|\Psi(t)\rangle = \hat{H}(t)|\Psi(t)\rangle$ is solved by numerical exponentiation of the Hamiltonian matrix (see Expokit [52]), and a detailed description of our numerical scheme can be found in [48]. In our simulations, the computational basis included all the rotational states with an angular momentum $J \leq 44$. For the case of propylene oxide molecules which is used as an example, at a temperature of $T = 5\text{K}$, initial states with $J \leq 8$ are included in the thermal averaging.

Classical simulation. In the classical limit, chiral molecules are modeled as asymmetric tops driven by an external torque. The classical equations of motion for the angular velocities (written in the frame of principal axes of inertia tensor) are the Euler's equations [53]

$$\mathbf{I}\dot{\boldsymbol{\Omega}} = (\mathbf{I}\boldsymbol{\Omega}) \times \boldsymbol{\Omega} + \mathbf{T}, \quad (4)$$

where $\boldsymbol{\Omega} = (\Omega_a, \Omega_b, \Omega_c)$ is the angular velocity vector, $\mathbf{I} = \text{diag}(I_a, I_b, I_c)$ is the moment of inertia tensor, and $\mathbf{T} = (T_a, T_b, T_c)$ is the external torque vector. The external torque originates from the electric field, which is defined in the laboratory frame. In order to solve Eq. (4), a time-dependent relation between the molecular frame (the frame of principal axes of inertia) and the laboratory frame is required.

Such a relation can be established with the help of a time-dependent unit quaternion, which is used to parametrize the rotation of the rigid body. Quaternions extend complex numbers, and are defined as quadruples of real numbers, $q = (q_0, q_1, q_2, q_3)$. The relation between a vector \mathbf{x} in the molecular frame and a vector \mathbf{X} in the laboratory frame is given by a simple linear transformation $\mathbf{x} = Q(t)\mathbf{X}$, where $Q(t)$ is a 3×3 matrix composed of the quaternion's elements [54, 55]. The quaternion obeys the following equation of motion

$$\dot{q} = \frac{1}{2}q\boldsymbol{\Omega}, \quad (5)$$

where $\boldsymbol{\Omega} = (0, \boldsymbol{\Omega})$ is a pure quaternion and the quaternion multiplication rule is implied [54, 55]. Equations (4) and (5) are coupled via the torque, $\mathbf{T} = \boldsymbol{\mu} \times Q\mathbf{E}$, where $\boldsymbol{\mu}$ is the molecular dipole moment vector.

To simulate the behavior of a classical ensemble, we use the Monte Carlo approach. For each individual asymmetric top, we numerically solve the system of Eqs. (4) and (5). We use ensembles consisting of $N = 10^7$ molecules, which are initially isotropically distributed in space, and the initial angular velocities are given by the Boltzmann distribution

$$P(\boldsymbol{\Omega}) \propto \exp\left(-\frac{\boldsymbol{\Omega}^T \mathbf{I} \boldsymbol{\Omega}}{2k_B T}\right) = \prod_i \exp\left(-\frac{I_i \Omega_i^2}{2k_B T}\right), \quad (6)$$

where T is the temperature and k_B is the Boltzmann constant. The initial uniform random quaternions were generated using the recipe described in [56].

III. RESULTS

We consider propylene oxide (referred to as PPO hereafter) as a typical example of a chiral molecule. Table I summarizes the molecular properties of the right-handed enantiomer, (*R*)-PPO. Molecular moments of inertia and

Molecule	Moments of inertia	Molecular dipole components
(<i>R</i>)-propylene oxide	$I_a = 180386$	$\mu_a = 0.965$
	$I_b = 493185$	$\mu_b = -1.733$
	$I_c = 553513$	$\mu_c = 0.489$

TABLE I. Molecular properties of (*R*)-PPO: eigenvalues of the moment of inertia tensor (in atomic units) and components of dipole moment (in Debye) in the frame of molecular principal axes of inertia.

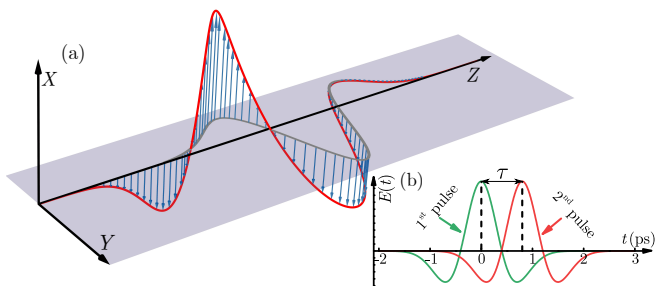


FIG. 1. (a) Illustration of the electric field with twisted polarization composed of two delayed cross-polarized THz pulses [see Eq. (7)]. The vertical blue arrows represent the X -projection of the field. The gray line in the YZ plane represents the Y -projection of the field. (b) Amplitude of the X -polarized (green) and the Y -polarized (red) pulses. Time dependence of the first pulse is given by $f(t) = (1 - 2at^2)e^{-at^2}$, while that of the second pulse by $f(t - \tau)$. Here, $a = 3.06 \text{ ps}^{-2}$ and $\tau = 0.80 \text{ ps}$. Time integral of the electric field is identically zero.

the components of molecular dipole moments were computed with the help of the GAUSSIAN software package (CAM-B3LYP/aug-cc-pVTZ method) [57].

The molecules are excited by a pair of delayed cross-polarized THz pulses. The combined electric field of the pulses is modeled using [45]

$$\mathbf{E}(t) = E_0 [f(t)\mathbf{e}_X + f(t - \tau)\mathbf{e}_Y], \quad (7)$$

where E_0 is the peak amplitude, $f(t) = (1 - 2at^2)e^{-at^2}$ defines the time dependence of each pulse, a determines the temporal width of the pulse, τ is the time delay between the peaks of the two pulses, and \mathbf{e}_X and \mathbf{e}_Y are the unit vectors along the laboratory X and Y axes, respectively. The pulses propagate along the laboratory Z axis, while \mathbf{E} twists in the XY plane, as shown in Fig. 1.

Figure 2 shows the dipole moment projections along the three laboratory axes, $\langle \mu_X \rangle$, $\langle \mu_Y \rangle$, and $\langle \mu_Z \rangle$, as functions of time. The angle brackets $\langle \cdot \rangle$ denote the incoherent average of initial thermally populated rotational states, or the ensemble average in the classical case. The parameters of the field are $a = 3.06 \text{ ps}^{-2}$, $\tau = 0.80 \text{ ps}$, and $E_0 = 8.0 \text{ MV/cm}$ (corresponding to the peak intensity of $8.5 \times 10^{10} \text{ W/cm}^2$), see Eq. (7) and Fig. 1. Note that THz pulses with peak amplitudes of tens of MV/cm, especially with the use of field enhancement structures [58–60], are experimentally available. It is evident from the insets in Fig. 2 that on the short time scale the classical and quantum results are in excellent agreement. Each of the THz pulses is followed by a splash of dipole signal in the direction of the pulse polarization, i.e. initially along the X axis, and then along the Y axis [see the minima in the insets of Figs. 2(a) and 2(b), which are before and after 0 ps, respectively]. This transient orientation induced by single THz pulses is expected and has been observed before [41–48].

However, an unexpected result emerges: a dipole projection along the Z axis (perpendicular to the plane of

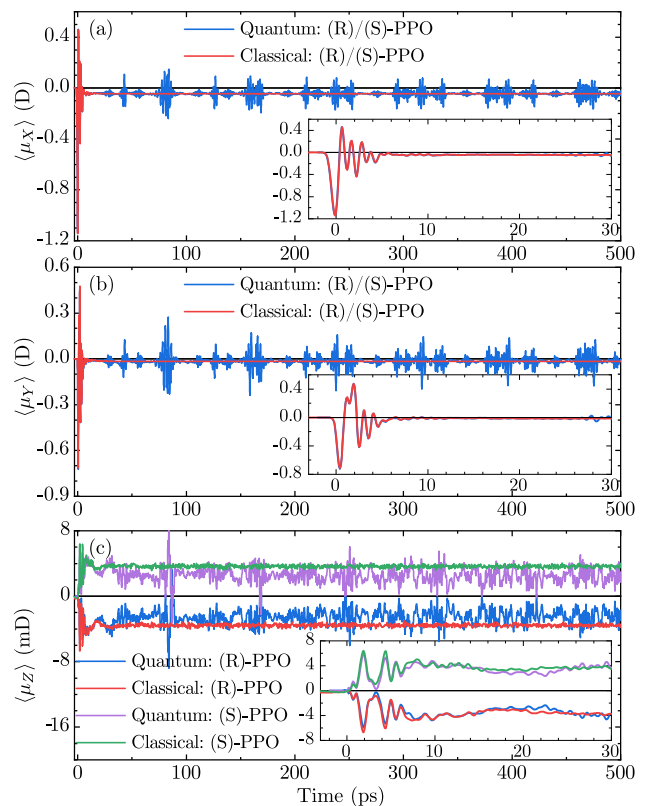


FIG. 2. Projections of the molecular dipole moment on the laboratory-fixed axes. The classical results (red and green) are ensemble averages, while quantum results (blue and purple) are incoherent averages over the initial thermally populated rotational states. Here $T = 5 \text{ K}$, and the THz field parameters are similar to Fig. 1, with $E_0 = 8.0 \text{ MV/cm}$. The insets show the magnified portions of the plots during the first 30 ps.

polarization twisting) appears after the second pulse [see Fig. 2(c)]. This orientation which is unique to chiral molecules is enantioselective, in the sense that the sign of the projection is opposite for the two enantiomers, positive for (S)-PPO and negative for (R)-PPO. The enantioselectivity of the orientation in the Z direction can be formally derived as well [for details, see Appendix A]. Similar enantioselective orientation was observed in chiral molecules optically excited by laser fields with twisted polarization acting on the molecular polarizability [21, 22, 24].

Furthermore, the classical results clearly show another remarkable feature of the induced orientation. After the field is switched off [$t > 2.5 \text{ ps}$, see Fig. 1(b)], the dipole projections along all three laboratory axes persist on the nanosecond timescale. The direct quantum simulation deviates from the classical one on the long time scale, exhibiting quantum beats/revivals [61–63]. Nevertheless, as can be seen from Fig. 3, on a timescale of 0.5 ns the time-averaged quantum signals reproduce well the steady state dipole signals obtained by the classical calculation.

Classically, the persistent long-term orientation shown

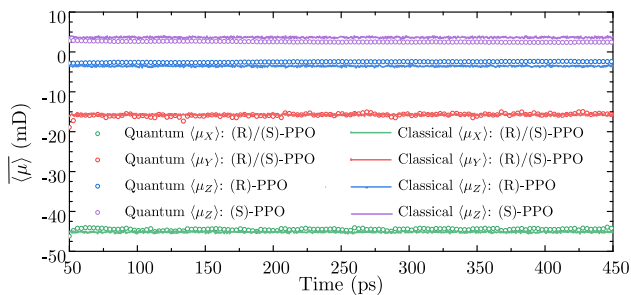


FIG. 3. Long-term behavior of the dipole projections shown in Fig. 2. Open circles represent sliding time average of the dipole signals $\langle \mu_X \rangle$ (green), $\langle \mu_Y \rangle$ (red), and $\langle \mu_Z \rangle$ (blue and purple) calculated quantum mechanically. The sliding time average is evaluated according to $\overline{\langle \mu_i \rangle}(t) = (\Delta t)^{-1} \int_{t-\Delta t/2}^{t+\Delta t/2} dt' \langle \mu_i \rangle(t')$, where $\Delta t = 100$ ps. For comparison, the correspondingly colored solid lines are the classical results.

in Figs. 2 and 3 is in fact permanent. In the absence of external torques (external fields), in the laboratory frame the angular momentum vector is conserved, while in the molecular frame the angular momentum follows a fixed trajectory, which can be visualized using the Binet construction [53]. Although the absolute orientation of an asymmetric top in the laboratory frame never recurs, depending on the energy and magnitude of the angular momentum, the projections of the molecular principal axes a or c on the conserved angular momentum vector have a constant sign [53]. As a result, the attained asymptotic values of the orientation factors do not change after the initial dephasing of the ensemble which, according to Fig. 2, takes about 30 ps. On the other hand, quantum mechanically, the notion of well-defined trajectories is invalid, which means that the orientation is simply *long-lived* and eventually will change its sign. Since the kinetic energy Hamiltonian [see Eq. (3)] couples rotational states with different K quantum number, the quantum-mechanical asymmetric top does not have permanently oriented eigenstates. Any initially oriented state will eventually oscillate between being oriented and anti-oriented, an effect known as dynamical tunneling [64]. Formally, for a quantum mechanical chiral rotor, one would expect no permanent orientation after the turn-off of all external fields. However, as we show here and as was shown in [23, 25], the tunneling timescale may exceed the excitation timescale by orders of magnitude.

Notice, the persistent orientation appearing in the directions of each of the pulses (along the X and Y axes) does not rely on chirality. It was recently shown that single THz pulses applied to symmetric- and asymmetric-top molecules also induce persistent orientation [48]. In contrast, both the appearance and permanency of the orientation along the propagation direction which is perpendicular to both the X and Y axes depend on the chirality of the molecule. Specifically, these effects rely

on the lack of molecular symmetry, i.e. all three molecular dipole moment components must differ from zero, $\mu_a, \mu_b, \mu_c \neq 0$ [see Appendix B]. For comparison, in the case of optical excitation by the laser fields with twisted polarization, the orientation relies on the existence of the off-diagonal elements of the polarizability tensor, which is a property of chiral molecules as well. In that case, the *induced dipole* has nonzero projections along all three principal axes, even when the laser field is polarized along only one of the molecular principal axes.

The magnitude of the THz-induced orientation is sensitive to the initial temperature and external field parameters [47, 48, 65, 66]. Through our classical simulations, we carried out an extensive study of the permanent orientation dependence on temperature, T , and the time delay between the two cross-polarized pulses, τ [see Eq. (7)]. The results are summarized in Fig. 4. The permanent values of the dipole projections (denoted by $\langle \mu_X \rangle_p$, $\langle \mu_Y \rangle_p$, and $\langle \mu_Z \rangle_p$) were obtained by following the field-free dynamics for a sufficiently long time until a steady-state is reached (typically $t > 100$ ps). Figure 4 shows that for a given rotational temperature, there are one or several disjoint ranges of τ resulting in optimal (largest absolute value) orientation. In general, the optimal time delay between the pulses is shorter for higher temperatures. Note, however, that the temperature dependence of the individual projections $\langle \mu_X \rangle_p$, $\langle \mu_Y \rangle_p$, and $\langle \mu_Z \rangle_p$ is non-monotonic. For example, at a fixed time delay $\tau \approx 0.5$ ps, $|\langle \mu_Z \rangle_p|$ increases with temperature up to $T \approx 120$ K, after which $|\langle \mu_Z \rangle_p|$ begins to decrease.

IV. CONCLUSIONS

We theoretically demonstrated a qualitatively new phenomenon of field-free enantioselective orientation of chiral molecules induced by THz pulses with twisted polarization. The twisted pulse induces orientations along the polarization directions of the two pulses forming the twisted pulse, and this orientation is of the same sign for both enantiomers. In the direction perpendicular to the polarization direction of both pulses, we find that the orientation is of opposite sign for the two enantiomers. The latter effect relies on the molecular chirality, namely on the lack of molecular symmetry, such that the molecular dipole has nonzero projections on all three molecular principal axes. The orientation was shown to persist long after the end of the pulses. We studied the dependence of persistent orientation values on the temperature and the time delay between the two cross-polarized THz pulses. The orientation factors were found to be quite robust against the detrimental effects of temperature provided that the time delay is adjusted appropriately. The orientation dynamics on timescales beyond nanoseconds requires a more detailed analysis, as other effects such as collisions and fine structure effects [67] become important in addition to dynamical tunneling. The relative importance of such effects should be assessed in future works.

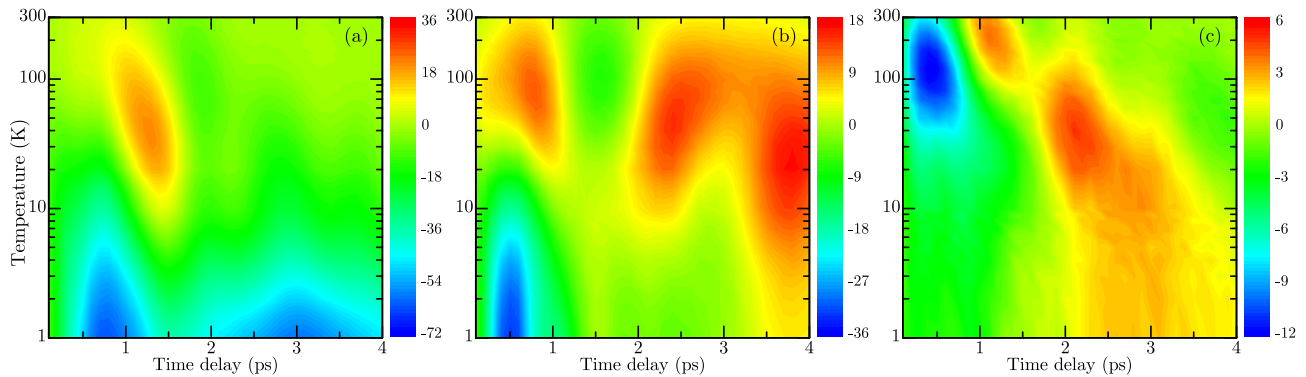


FIG. 4. Classically calculated permanent values of the dipole signals (a) $\langle \mu_X \rangle_p$, (b) $\langle \mu_Y \rangle_p$, and (c) $\langle \mu_Z \rangle_p$ as functions of temperature, T , and time delay between the two THz pulses, τ . The color scales are in the units of millidebye (mD).

The orientation persisting on the nanosecond timescale may be measured by means of second (or higher order) harmonic generation [68], and could be used for deflection by inhomogeneous electric fields [69, 70] (for an extensive review, see [71]). The enantioselective orientation along the propagation direction may be useful for fast and precise analysis of enantiomeric excess, and may facilitate *enantioselective* separation using inhomogeneous fields [72]. In the past [20–25], related effects induced by optical pulses with twisted polarizations have been reported, and further exploration will examine the combined effect of THz and optical fields together that could maximize the difference in orientations between the two enantiomers.

ACKNOWLEDGMENTS

I.A. gratefully acknowledges support by the Israel Science Foundation (Grant No. 746/15). K.A.N. acknowledges support by the U.S. National Science Foundation Grant CHE-1665383. I.A. acknowledges support as the Patricia Elman Bildner Professorial Chair. This research was made possible in part by the historic generosity of the Harold Perlman Family.

Appendix A: Qualitative demonstration of enantioselective orientation

Consider two overlapping THz pulses propagating along the laboratory Z axis, and which are polarized

along X and Y axes, respectively. The nonzero matrix elements of the interaction potential can be written as

$$\begin{aligned} & \langle JKM | \hat{H}_{\text{int}}(t) | J', K-s, M-p \rangle \\ &= \mu_s^{(1)} E_{-p}^{(1)}(t) \langle JKM | D_{p,s}^{1*}(R) | J', K-s, M-p \rangle, \end{aligned} \quad (\text{A1})$$

where $s = 0, \pm 1$, and $p = \pm 1$ (since $E_0^{(1)} = 0$). Here $\mu_s^{(1)}$ and $E_p^{(1)}$ are the dipole moment and electric field, respectively, expressed as spherical tensors of rank 1, with components $\mu_{\pm 1}^{(1)} = \mp(\mu_b \pm i\mu_c)/\sqrt{2}$, $\mu_0^{(1)} = \mu_a$, and $E_{\pm 1}^{(1)} = \mp(E_X \pm iE_Y)/\sqrt{2}$, $E_0^{(1)} = E_Z$. $D_{p,s}^{1*}(R)$ is the complex conjugate of the Wigner D-matrix, where R denotes the set of the three Euler angles, (θ, ϕ, χ) .

The THz pulses induce dynamics of the Z -component of the polarization, defined by

$$P_Z(t) = \sum_{s=-1}^{+1} \mu_s^{(1)} \langle \Psi(t) | D_{0,s}^{1*}(R) | \Psi(t) \rangle, \quad (\text{A2})$$

where the wave function is given by $|\Psi(t)\rangle = \hat{U}(t,0)|\Psi(0)\rangle$, with $\hat{U}(t,0)$ being the evolution operator. Since the discussion here is qualitative, for simplicity we assume that initially the rotor is in the ground rotational state $|JKM\rangle = |000\rangle$, such that $|\Psi(t)\rangle = \hat{U}(t,0)|000\rangle$.

The evolution operator, $\hat{U}(t,0)$ can be expanded in a Dyson series

$$\hat{U}(t,0) = \sum_{n=0}^{\infty} \frac{(-i)^n}{n!} \int_0^t dt_1 \int_0^{t_1} dt_2 \cdots \int_0^{t_{n-1}} dt_n \hat{T} \hat{H}_{\text{int}}(t_1) \hat{H}_{\text{int}}(t_2) \cdots \hat{H}_{\text{int}}(t_n), \quad (\text{A3})$$

where \hat{T} is the time-ordering operator. From the properties of Wigner 3-j symbols it follows that the only non-zero matrix elements, $\langle JKM | D_{0,s}^{1*}(R) | J', K-s, M \rangle \neq 0$, are those satisfying $|J-1| \leq J' \leq J+1$. Hence, the nonzero

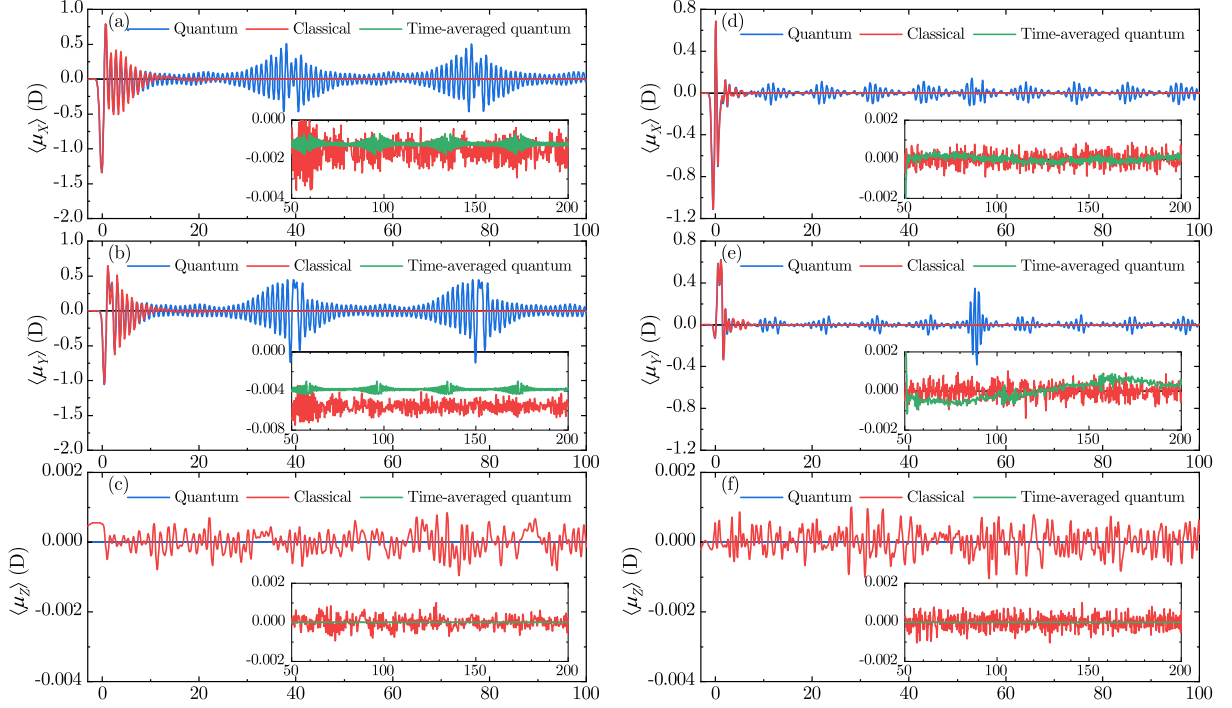


FIG. 5. Thermally averaged X, Y, Z -projections of the dipole moment in the laboratory frame, $\langle \mu_X \rangle$, $\langle \mu_Y \rangle$, and $\langle \mu_Z \rangle$ as functions of time for (a-c) CH₃Cl and (d-f) SO₂ molecules. The results of quantum and classical simulations are shown in blue and red lines, respectively. The green curve represents the sliding time average defined by $\langle \mu_i \rangle(t) = (\Delta t)^{-1} \int_{t-\Delta t/2}^{t+\Delta t/2} dt' \langle \mu_i \rangle(t')$, where (a-c) $\Delta t = 38.2$ ps and (d-f) $\Delta t = 100$ ps, respectively. The insets show a magnified portion of the signals.

components of polarization are

$$\begin{aligned}
 V_s &\sim \mu_s^{(1)} \langle \prod_n \hat{H}_{\text{int}}(t_n) 000 | D_{0,s}^{1*}(R) | \prod_{n'} \hat{H}_{\text{int}}(t'_{n'}) 000 \rangle \\
 &= \mu_s^{(1)} \sum_{J'_1 J_1 K_1 M_1} \langle \prod_n \hat{H}_{\text{int}}(t_n) 000 | J_1 K_1 M_1 \rangle \langle J_1 K_1 M_1 | D_{0,s}^{(1)*} | J'_1, K_1 - s, M_1 \rangle \langle J'_1, K_1 - s, M_1 | \prod_{n'} \hat{H}_{\text{int}}(t'_{n'}) 000 \rangle. \quad (\text{A4})
 \end{aligned}$$

Note that for the qualitative argument here, the evolution operator in Eq. (A4) is considered as $\hat{U}(t, 0) \sim \prod_n \hat{H}_{\text{int}}(t_n)$. From Eq. (A4), we know that V_s differs from zero only if $\langle J_1 + J'_1, 2K_1 - s, 2M_1 | \prod_n \hat{H}_{\text{int}}(t_n) \prod_{n'} \hat{H}_{\text{int}}(t'_{n'}) | 000 \rangle \neq 0$. Also, according to Eq. (A1), the allowed transitions are between the states with M and $M \pm 1$, because $p = \pm 1$. Hence, it follows from Eq. (A4) that the state changing from 0 to $2M_1$ involves an even number of interaction terms (\hat{H}_{int}). Similarly, transitions between states with K quantum number equals 0 and $2K_1 - s$ involve $2l + s$ interaction terms with $s = 0$ [see Eq. (A1), with $s = 0$] and $2L + s$ interaction terms with $s = \pm 1$ [see Eq. (A1), with $s = \pm 1$], where L and l are integers. The dipole moments of two enantiomers of the chiral molecule satisfy $\mu_{\pm 1}^{(S)} = \mu_{\pm 1}^{(R)}$ and $\mu_0^{(S)} = -\mu_0^{(R)}$, such that the non-zero polarization

components [see Eq. (A4)] satisfy

$$\begin{aligned}
 \frac{V_s^{(S)}}{V_s^{(R)}} &= \frac{\mu_s^{(S)}}{\mu_s^{(R)}} \left(\frac{\mu_{-1}^{(S)}}{\mu_{-1}^{(R)}} \right)^{L'} \left(\frac{\mu_0^{(S)}}{\mu_0^{(R)}} \right)^{2l+s} \left(\frac{\mu_1^{(S)}}{\mu_1^{(R)}} \right)^{2L+s-L'} \\
 &= \frac{\mu_s^{(S)}}{\mu_s^{(R)}} \left(\frac{\mu_0^{(S)}}{\mu_0^{(R)}} \right)^s = -1, \quad (\text{A5})
 \end{aligned}$$

where $s = 0, \pm 1$, and L' is an integer. As one can see, the components of polarization of the two enantiomers are of opposite signs, and thereby the polarizations satisfy $P_Z^{(S)}(t) = -P_Z^{(R)}(t)$.

Appendix B: Orientation of non-chiral molecules

Figure 5 shows the orientation signals along the three laboratory axes, $\langle \mu_X \rangle(t)$, $\langle \mu_Y \rangle(t)$, and $\langle \mu_Z \rangle(t)$, for two non-chiral molecules. The first one is the symmetric-top methyl chloride (CH_3Cl), in which the molecular dipole moment is along the symmetry axis, a axis ($\mu_b = \mu_c = 0$, see Table II). The second molecule, sulfur dioxide (SO_2) is an asymmetric-top molecule in which the molecular dipole moment is along the molecular b axis ($\mu_a = \mu_c = 0$, see Table II). The parameters of the THz pulses are similar to Fig. 2. The initial temperature is $T = 5$ K. The quantum and classical results are in good agreement. As expected, both the symmetric- [Figs. 5(a) and 5(b)] and non-chiral asymmetric-top [Figs. 5(d) and 5(e)] molecules immediately respond to the X -polarized and Y -polarized pulses. However, in contrast to chiral molecules [see Fig. 2], the Z -projection of the dipole moment remains zero [see Figs. 5(c) and 5(f)]. Note that $\langle \mu_Z \rangle$ calculated quantum mechanically is identically zero, while the small amplitude oscillations appearing in the classical results are due to the finite number (N)

of molecules in the ensemble. The lack of orientation in the cases of symmetric- or non-chiral asymmetric-top molecules indicates that all three molecular dipole components (μ_a, μ_b, μ_c) are indeed required for inducing the perpendicular (in the Z direction) orientation. Other combinations were considered numerically as well (not shown), e.g. asymmetric top molecule having two non-zero molecular dipole components. In all cases, there is no perpendicular orientation, i.e. $\langle \mu_Z \rangle = 0$.

Molecule	Moments of inertia	Molecular dipole components
methyl chloride	$I_a = 20910$	$\mu_a = 1.986$
	$I_b = 251506$	$\mu_b = 0$
	$I_c = 251506$	$\mu_c = 0$
sulfur dioxide	$I_a = 57812$	$\mu_a = 0$
	$I_b = 323141$	$\mu_b = -1.805$
	$I_c = 380953$	$\mu_c = 0$

TABLE II. Molecular properties of methyl chloride (CH_3Cl) and sulfur dioxide (SO_2) molecules: eigenvalues of the moment of inertia tensor (in atomic units) and components of dipole moment (in Debye) in the frame of molecular principal axes of inertia.

-
- [1] L. Pasteur, Sur les relations qui peuvent exister entre la forme cristalline, la composition chimique et le sens de la polarisation rotatoire, *Ann. Phys. Chem.* **24**, 442 (1848).
- [2] S. F. Mason, The foundations of classical stereochemistry, in *Topics in Stereochemistry* (John Wiley & Sons, Ltd, 2007) pp. 1–34.
- [3] F. A. Cotton, *Chemical Applications of Group Theory*, 3rd ed. (John Wiley and Sons, New York, 1990).
- [4] R. Berger and J. Stohner, Parity violation, *Wiley Interdiscip. Rev. Comput. Mol. Sci* **9**, e1396 (2019).
- [5] D. Patterson, M. Schnell, and J. M. Doyle, Enantiomer-specific detection of chiral molecules via microwave spectroscopy, *Nature* **497**, 475 (2013).
- [6] D. Patterson and J. M. Doyle, Sensitive Chiral Analysis via Microwave Three-Wave Mixing, *Phys. Rev. Lett.* **111**, 023008 (2013).
- [7] D. Patterson and M. Schnell, New studies on molecular chirality in the gas phase: enantiomer differentiation and determination of enantiomeric excess, *Phys. Chem. Chem. Phys.* **16**, 11114 (2014).
- [8] V. A. Shubert, D. Schmitz, and M. Schnell, Enantiomer-sensitive spectroscopy and mixture analysis of chiral molecules containing two stereogenic centers – microwave three-wave mixing of menthone, *J. Mol. Spectrosc.* **300**, 31 (2014).
- [9] K. K. Lehmann, Theory of Enantiomer-Specific Microwave Spectroscopy, in *Frontiers and Advances in Molecular Spectroscopy* (Elsevier, 2018) pp. 713–743.
- [10] M. Leibscher, T. F. Giesen, and C. P. Koch, Principles of enantio-selective excitation in three-wave mixing spectroscopy of chiral molecules, *J. Chem. Phys.* **151**, 014302 (2019).
- [11] B. Ritchie, Theory of the angular distribution of photoelectrons ejected from optically active molecules and molecular negative ions, *Phys. Rev. A* **13**, 1411 (1976).
- [12] N. Böwering, T. Lischke, B. Schmidtke, N. Müller, T. Khalil, and U. Heinzmann, Asymmetry in Photoelectron Emission from Chiral Molecules Induced by Circularly Polarized Light, *Phys. Rev. Lett.* **86**, 1187 (2001).
- [13] C. Lux, M. Wollenhaupt, T. Bolze, Q. Liang, J. Köhler, C. Sarpe, and T. Baumert, Circular Dichroism in the Photoelectron Angular Distributions of Camphor and Fenchone from Multiphoton Ionization with Femtosecond Laser Pulses, *Angew. Chem. Int. Ed. Engl.* **51**, 5001 (2012).
- [14] S. Beaulieu, A. Comby, A. Clergerie, J. Caillat, D. Descamps, N. Dudovich, B. Fabre, R. Géneaux, F. Légaré, S. Petit, B. Pons, G. Porat, T. Ruchon, R. Taïeb, V. Blanchet, and Y. Mairesse, Attosecond-resolved photoionization of chiral molecules, *Science* **358**, 1288 (2017).
- [15] S. Beaulieu, A. Comby, D. Descamps, B. Fabre, G. A. Garcia, R. Géneaux, A. G. Harvey, F. Légaré, Z. Masín, L. Nahon, A. F. Ordóñez, S. Petit, B. Pons, Y. Mairesse, O. Smirnova, and V. Blanchet, Photoexcitation circular dichroism in chiral molecules, *Nat. Phys.* **14**, 484 (2018).
- [16] M. Pitzer, M. Kunitski, A. S. Johnson, T. Jahnke, H. Sann, F. Sturm, L. P. H. Schmidt, H. Schmidt-Böcking, R. Dörner, J. Stohner, J. Kiedrowski, M. Reggelin, S. Marquardt, A. Schießler, R. Berger, and M. S. Schöffler, Direct Determination of Absolute Molecular Stereochemistry in Gas Phase by Coulomb Explosion Imaging, *Science* **341**, 1096 (2013).
- [17] P. Herwig, K. Zawatzky, M. Grieser, O. Heber, B. Jordon-Thaden, C. Krantz, O. Novotný, R. Repnow, V. Schurig, D. Schwalm, Z. Vager, A. Wolf, O. Trapp, and

- H. Kreckel, Imaging the Absolute Configuration of a Chiral Epoxide in the Gas Phase, *Science* **342**, 1084 (2013).
- [18] K. Fehre, S. Eckart, M. Kunitski, M. Pitzer, S. Zeller, C. Janke, D. Trabert, J. Rist, M. Weller, A. Hartung, L. P. H. Schmidt, T. Jahnke, R. Berger, R. Dörner, and M. S. Schöffler, Enantioselective fragmentation of an achiral molecule in a strong laser field, *Sci. Adv.* **5**, eaau7923 (2019).
- [19] R. Cireasa, A. E. Boguslavskiy, B. Pons, M. C. H. Wong, D. Descamps, S. Petit, H. Ruf, N. Thiré, A. Ferré, J. Suarez, J. Higuete, B. E. Schmidt, A. F. Alharbi, F. Légaré, V. Blanchet, B. Fabre, S. Patchkovskii, O. Smirnova, Y. Mairesse, and V. R. Bhardwaj, Probing molecular chirality on a sub-femtosecond timescale, *Nat. Phys.* **11**, 654 (2015).
- [20] A. Yachmenev and S. N. Yurchenko, Detecting Chirality in Molecules by Linearly Polarized Laser Fields, *Phys. Rev. Lett.* **117**, 033001 (2016).
- [21] E. Gershnel and I. Sh. Averbukh, Orienting Asymmetric Molecules by Laser Fields with Twisted Polarization, *Phys. Rev. Lett.* **120**, 083204 (2018).
- [22] I. Tutunnikov, E. Gershnel, S. Gold, and I. Sh. Averbukh, Selective Orientation of Chiral Molecules by Laser Fields with Twisted Polarization, *J. Phys. Chem. Lett.* **9**, 1105 (2018).
- [23] I. Tutunnikov, J. Floß, E. Gershnel, P. Brumer, and I. Sh. Averbukh, Laser-induced persistent orientation of chiral molecules, *Phys. Rev. A* **100**, 043406 (2019).
- [24] A. A. Milner, J. A. M. Fordyce, I. MacPhail-Bartley, W. Wasserman, V. Milner, I. Tutunnikov, and I. Sh. Averbukh, Controlled Enantioselective Orientation of Chiral Molecules with an Optical Centrifuge, *Phys. Rev. Lett.* **122**, 223201 (2019).
- [25] I. Tutunnikov, J. Floß, E. Gershnel, P. Brumer, I. Sh. Averbukh, A. A. Milner, and V. Milner, Observation of persistent orientation of chiral molecules by a laser field with twisted polarization, *Phys. Rev. A* **101**, 021403 (2020).
- [26] S. Fleischer, Y. Khodorkovsky, Y. Prior, and I. Sh. Averbukh, Controlling the sense of molecular rotation, *New J. Phys.* **11**, 105039 (2009).
- [27] K. Kitano, H. Hasegawa, and Y. Ohshima, Ultrafast Angular Momentum Orientation by Linearly Polarized Laser Fields, *Phys. Rev. Lett.* **103**, 223002 (2009).
- [28] Y. Khodorkovsky, K. Kitano, H. Hasegawa, Y. Ohshima, and I. Sh. Averbukh, Controlling the sense of molecular rotation: Classical versus quantum analysis, *Phys. Rev. A* **83**, 023423 (2011).
- [29] S. Zhdanovich, A. A. Milner, C. Bloomquist, J. Floß, I. Sh. Averbukh, J. W. Hepburn, and V. Milner, Control of Molecular Rotation with a Chiral Train of Ultrashort Pulses, *Phys. Rev. Lett.* **107**, 243004 (2011).
- [30] J. Floß and I. Sh. Averbukh, Molecular spinning by a chiral train of short laser pulses, *Phys. Rev. A* **86**, 063414 (2012).
- [31] Y. Kida, S.-i. Zaitso, and T. Imasaka, Stimulated rotational Raman scattering by a polarization-modulated femtosecond pulse, *Phys. Rev. A* **77**, 063802 (2008).
- [32] Y. Kida, S.-i. Zaitso, and T. Imasaka, Coherent molecular rotations induced by a femtosecond pulse consisting of two orthogonally polarized pulses, *Phys. Rev. A* **80**, 021805(R) (2009).
- [33] G. Karras, M. Ndong, E. Hertz, D. Sugny, F. Billard, B. Lavorel, and O. Faucher, Polarization Shaping for Unidirectional Rotational Motion of Molecules, *Phys. Rev. Lett.* **114**, 103001 (2015).
- [34] E. Prost, H. Zhang, E. Hertz, F. Billard, B. Lavorel, P. Bejot, J. Zyss, I. Sh. Averbukh, and O. Faucher, Third-order-harmonic generation in coherently spinning molecules, *Phys. Rev. A* **96**, 043418 (2017).
- [35] K. Mizuse, N. Sakamoto, R. Fujimoto, and Y. Ohshima, Direct imaging of direction-controlled molecular rotational wave packets created by a polarization-skewed double-pulse, *Phys. Chem. Chem. Phys.* **22**, 10853 (2020).
- [36] J. Karczmarek, J. Wright, P. Corkum, and M. Ivanov, Optical Centrifuge for Molecules, *Phys. Rev. Lett.* **82**, 3420 (1999).
- [37] D. M. Villeneuve, S. A. Aseyev, P. Dietrich, M. Spanner, M. Y. Ivanov, and P. B. Corkum, Forced Molecular Rotation in an Optical Centrifuge, *Phys. Rev. Lett.* **85**, 542 (2000).
- [38] L. Yuan, S. W. Teitelbaum, A. Robinson, and A. S. Mullin, Dynamics of molecules in extreme rotational states, *Proc. Natl. Acad. Sci. U.S.A.* **108**, 6872 (2011).
- [39] A. Korobenko, A. A. Milner, and V. Milner, Direct Observation, Study, and Control of Molecular Superrotors, *Phys. Rev. Lett.* **112**, 113004 (2014).
- [40] A. Korobenko, Control of molecular rotation with an optical centrifuge, *J. Phys. B* **51**, 203001 (2018).
- [41] S. Fleischer, Y. Zhou, R. W. Field, and K. A. Nelson, Molecular Orientation and Alignment by Intense Single-Cycle THz Pulses, *Phys. Rev. Lett.* **107**, 163603 (2011).
- [42] K. Kitano, N. Ishii, N. Kanda, Y. Matsumoto, T. Kanai, M. Kuwata-Gonokami, and J. Itatani, Orientation of jet-cooled polar molecules with an intense single-cycle THz pulse, *Phys. Rev. A* **88**, 061405 (2013).
- [43] K. N. Egodapitiya, S. Li, and R. R. Jones, Terahertz-Induced Field-Free Orientation of Rotationally Excited Molecules, *Phys. Rev. Lett.* **112**, 103002 (2014).
- [44] P. Babilotte, K. Hamraoui, F. Billard, E. Hertz, B. Lavorel, O. Faucher, and D. Sugny, Observation of the field-free orientation of a symmetric-top molecule by terahertz laser pulses at high temperature, *Phys. Rev. A* **94**, 043403 (2016).
- [45] L. H. Coudert, Optimal orientation of an asymmetric top molecule with terahertz pulses, *J. Chem. Phys.* **146**, 024303 (2017).
- [46] R. Damari, D. Rosenberg, and S. Fleischer, Coherent Radiative Decay of Molecular Rotations: A Comparative Study of Terahertz-Oriented versus Optically Aligned Molecular Ensembles, *Phys. Rev. Lett.* **119**, 033002 (2017).
- [47] R. Tehini, K. Hamraoui, and D. Sugny, Shaping of the time evolution of field-free molecular orientation by THz laser pulses, *Phys. Rev. A* **99**, 033419 (2019).
- [48] L. Xu, I. Tutunnikov, E. Gershnel, Y. Prior, and I. Sh. Averbukh, Long-Lasting Molecular Orientation Induced by a Single Terahertz Pulse, *Phys. Rev. Lett.* **125**, 013201 (2020).
- [49] R. V. Krems, *Molecules in Electromagnetic Fields: From Ultracold Physics to Controlled Chemistry* (Wiley, 2018).
- [50] C. P. Koch, M. Lemeshko, and D. Sugny, Quantum control of molecular rotation, *Rev. Mod. Phys.* **91**, 035005 (2019).
- [51] R. N. Zare, *Angular momentum: understanding spatial aspects in chemistry and physics* (Wiley, New York, 1988).

- [52] R. B. Sidje, Expokit: A software package for computing matrix exponentials, *ACM Trans. Math. Softw.* **24**, 130 (1998).
- [53] H. Goldstein, C. Poole, and J. Safko, *Classical Mechanics* (Addison Wesley, San Francisco, CA, 2002).
- [54] E. A. Coutsias and L. Romero, The quaternions with an application to rigid body dynamics, Sandia Technical Report, SAND2004-0153 (2004).
- [55] J. B. Kuipers, *Quaternions and Rotation Sequences: A Primer with Applications to Orbits, Aerospace and Virtual Reality* (Princeton University Press, Princeton, N.J., 1999).
- [56] S. M. LaValle, *Planning Algorithms* (Cambridge University Press, New York, 2006).
- [57] M. J. Frisch, G. W. Trucks, H. B. Schlegel, G. E. Scuseria, M. A. Robb, J. R. Cheeseman, G. Scalmani, V. Barone, G. A. Petersson, H. Nakatsuji, X. Li, M. Caricato, A. V. Marenich, J. Bloino, B. G. Janesko, R. Gomperts, B. Mennucci, H. P. Hratchian, J. V. Ortiz, A. F. Izmaylov, *et al.*, Gaussian 16 Revision A. 03, Gaussian Inc. Wallingford CT (2016).
- [58] M. Clerici, M. Peccianti, B. E. Schmidt, L. Caspani, M. Shalaby, M. Giguère, A. Lotti, A. Couairon, F. m. c. Légaré, T. Ozaki, D. Faccio, and R. Morandotti, Wavelength Scaling of Terahertz Generation by Gas Ionization, *Phys. Rev. Lett.* **110**, 253901 (2013).
- [59] T. I. Oh, Y. J. Yoo, Y. S. You, and K. Y. Kim, Generation of strong terahertz fields exceeding 8 MV/cm at 1 kHz and real-time beam profiling, *Appl. Phys. Lett.* **105**, 041103 (2014).
- [60] D. Kuk, Y. J. Yoo, E. W. Rosenthal, N. Jhajj, H. M. Milchberg, and K. Y. Kim, Generation of scalable terahertz radiation from cylindrically focused two-color laser pulses in air, *Appl. Phys. Lett.* **108**, 121106 (2016).
- [61] I. Sh. Averbukh and N. F. Perelman, Fractional revivals: Universality in the long-term evolution of quantum wave packets beyond the correspondence principle dynamics, *Phys. Lett. A* **139**, 449 (1989).
- [62] P. M. Felker, Rotational Coherence Spectroscopy: Studies of the Geometries of Large Gas-Phase Species by Picosecond Time-Domain Methods, *J. Phys. Chem.* **96**, 7844 (1992).
- [63] R. Robinett, Quantum wave packet revivals, *Phys. Rep.* **392**, 1 (2004).
- [64] S. Keshavamurthy and P. Schlagheck, *Dynamical tunneling: theory and experiment* (CRC Press, Boca Raton, 2011).
- [65] M. Lapert and D. Sugny, Field-free molecular orientation by terahertz laser pulses at high temperature, *Phys. Rev. A* **85**, 063418 (2012).
- [66] C.-C. Shu and N. E. Henriksen, Field-free molecular orientation induced by single-cycle THz pulses: The role of resonance and quantum interference, *Phys. Rev. A* **87**, 013408 (2013).
- [67] E. F. Thomas, A. A. Søndergaard, B. Shepperson, N. E. Henriksen, and H. Stapelfeldt, Hyperfine-Structure-Induced Depolarization of Impulsively Aligned I₂ Molecules, *Phys. Rev. Lett.* **120**, 163202 (2018).
- [68] E. Frumker, C. T. Hebeisen, N. Kajumba, J. B. Bertrand, H. J. Wörner, M. Spanner, D. M. Villeneuve, A. Naumov, and P. B. Corkum, Oriented Rotational Wave-Packet Dynamics Studies via High Harmonic Generation, *Phys. Rev. Lett.* **109**, 113901 (2012).
- [69] E. Gershnel and I. Sh. Averbukh, Electric deflection of rotating molecules, *J. Chem. Phys.* **134**, 054304 (2011).
- [70] E. Gershnel and I. Sh. Averbukh, Deflection of rotating symmetric top molecules by inhomogeneous fields, *J. Chem. Phys.* **135**, 084307 (2011).
- [71] Y.-P. Chang, D. A. Horke, S. Trippel, and J. Küpper, Spatially-controlled complex molecules and their applications, *Int. Rev. Phys. Chem.* **34**, 557 (2015).
- [72] A. Yachmenev, J. Onvlee, E. Zak, A. Owens, and J. Küpper, Field-Induced Diastereomers for Chiral Separation, *Phys. Rev. Lett.* **123**, 243202 (2019).